JOURNAL OF GEOPHYSICAL RESEARCH, VOL. 111, C06034, doi:10.1029/2005JC003298, 2006



# Modeling South China Sea circulation: Response to seasonal forcing regimes

Jianping Gan,[1] H. Li,[1] E. N. Curchitser,[2] and D. B. Haidvogel[3]

Received 16 September 2005; revised 20 January 2006; accepted 13 March 2006; published 24 June 2006.

[1] A three-dimensional ocean model has been utilized to study circulation and its seasonal variation in the South China Sea (SCS) in response to the forcing of the Asian monsoon and the Kuroshio intrusion. The SCS ocean model has a resolution of approximately 10 km horizontal spacing and 30 vertical levels with a realistic bottom topography. The model is forced with time-dependent wind stress and heat flux from National Center for Environmental Prediction Reanalysis data as well as with lateral fluxes from a Pacific Ocean model of 40 km horizontal resolution. This study reports on the analysis of the mean seasonal circulation and dynamic processes in response to monsoonal wind stress, the Kuroshio intrusion, and other intrinsic forcing processes. It is found that the seasonal circulation in the SCS is mainly driven by the monsoonal wind stress and greatly influenced by the inflow from the Kuroshio intrusion. Strong currents along the continental margin of the SCS form mean basin-wide cyclonic and anticyclonic circulations in the winter and summer, respectively. Multiscale eddies are embedded in the general circulation across the basin. While mainstream of the Kuroshio passes through the Luzon Strait without intruding into the SCS, partial intrusion occurs in the upper 200 m near the shelf margin southwest of Taiwan at times when winter dynamic conditions prevail in the north SCS. The intrusion of the Kuroshio into the SCS also occurs at depths in all seasons, mainly along the continental slope. The coastal current separation to the east off southern Vietnam and the associated eddy formations characterize the circulation in the south SCS. The simulated results compare well with the corresponding observed fields. Dynamical processes involved in the forced flow fields are investigated by examination of the momentum balances. The analyses reveal that the circulation in the SCS is generally dominated by the geostrophic currents. North of the Luzon Strait, positive nonlinearity in the zonal direction is locally intensified, which leads to the formation of centripetal acceleration for the mainstream of the Kuroshio to turn eastward. The Kuroshio intrusion at depths is governed by the ageostrophic flows and highly associated with the net westward pressure gradient force. Coastal jet separation to the east off Vietnam is mainly associated with the local wind stress field and with the shelf topography in the summer and winter, respectively. Sensitivity study reveals that the weakening of the Kuroshio markedly enhances Kuroshio's intrusion and forms an anticyclonic eddy west of the Luzon Strait.

**Citation:** Gan, J., H. Li, E. N. Curchitser, and D. B. Haidvogel (2006), Modeling South China Sea circulation: Response to seasonal forcing regimes, *J. Geophys. Res.*, *111*, C06034, doi:10.1029/2005JC003298.

## 1. Introduction

[2] The South China Sea (SCS), a marginal sea of the western Pacific Ocean (Figure 1), is under strong influence by the Asian monsoon, characterized by prevailing northeasterly and southwesterly winds in winter and summer, respectively. Driven by the winter and summer monsoons, predominant basin-wide circulation in the upper layer is cyclonic and anticyclonic in the SCS, respectively [*Wyrtki*, 1961]. The winter/summer monsoon forms a southwestward/northeastward current over the broad continental shelves in the northern and western SCS and a northeastward/southwestward current in the part of deep basin (up to 5000 m). Eddies with different horizontal scales are embedded in the circulation [*Xu et al.*, 1982]. External fluxes from the adjacent open ocean also have significant impacts on the circulation in the SCS. On the eastern part of the basin, the SCS connects with the East China Sea through the Taiwan Strait and with the Pacific Ocean through the

[1]Department of Mathematics and Atmospheric, Marine and Coastal Environment Program, Hong Kong University of Science and Technology, Kowloon, Hong Kong.

[2]Lamont-Doherty Earth Observatory of Columbia University, Palisades, New York, USA.

[3]Institute of Marine and Coastal Sciences, Rutgers University, New Brunswick, New Jersey, USA.


0148-0227/06/2005JC003298$09.00

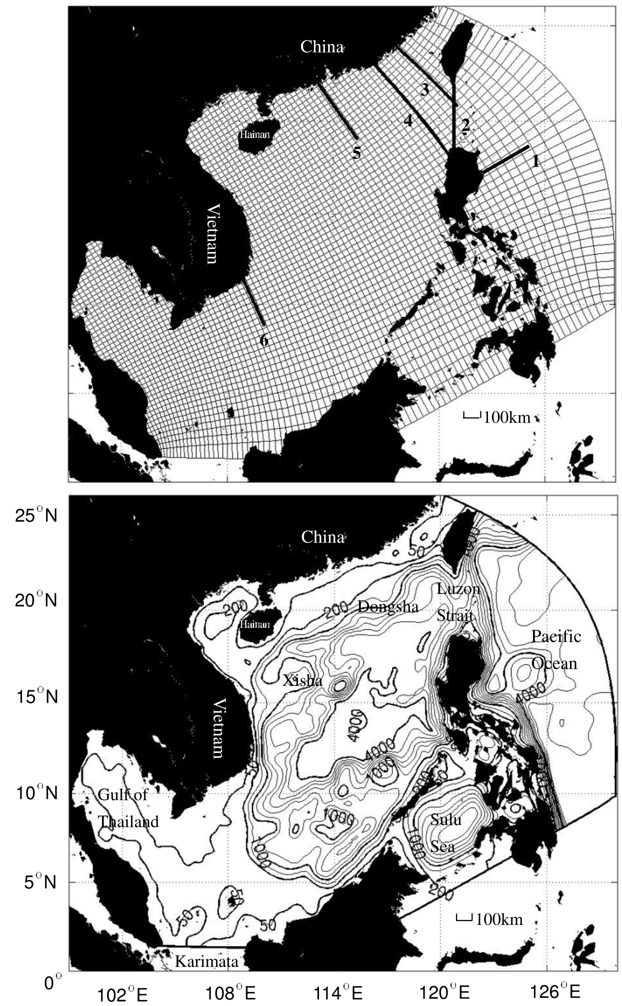


**Figure 1.** Model's curvilinear grid and bathymetry with the 50, 200, 500, 1000, and 4000 m isobaths shown as thicker lines. The contour interval for water deeper than 200 m is 500 m. One third of the horizontal grid point is shown. The locations of the cross sections are labeled with lines 1 to 6, representing the cross sections at the eastern Philippines (line 1), at the Luzon Strait (line 2), and at the locations normal to the coastline along the northern and western SCS (from lines 3–6).

Luzon Strait. On the southern boundary, it links with the Java Sea through the Karimata Strait on the west and with the Celebes Sea through the Sulu Sea on the east. In western Pacific, the North Equatorial Current (NEC) bifurcates on the east coast of the Philippines at about 15°N [*Qu and Lukas*, 2003]. The northward component of the bifurcated NEC intensifies the western boundary current, the Kuroshio (KU) and the southward component forms Mindanao current. The bifurcation location of NEC shifts northward and southward in winter and summer, respectively [*Yaremchuk and Qu*, 2005]. As KU passes through the Luzon Strait, it may turn westward and intrude into the SCS. The intrusion of the KU is expected to alter the wind-induced circulation in the SCS. It has been found [e.g., *Shaw*, 1991; *Shaw and Chao*, 1994 and *Xie et al.*, 2003] that the KU tends to intrude into the SCS during winter. On other occasions, the KU could form a loop current near the Luzon Strait [*Li and Wu*, 1989; *Farris and Wimbush*, 1996], in which KU typically enters (exits) from south (north) of the Luzon Strait without penetrating into the interior of the SCS. When the KU intrudes into the SCS, it could reach to the interior of the SCS along the continental margin and interact with the locally generated circulation. Waters from the KU were also found in the NSCS and along the west coast of Taiwan [*Shaw*, 1992]. A detailed review of the existing viewpoints about the KU intrusion has been presented by *Hu et al.* [2000]. The dynamics associated with KU and its intrusion, however, remain unclear despite its important role in the flow field in the SCS. Circulation in the south SCS (SSCS) is also important in characterizing the circulation pattern in the basin. The separation of the boundary current and associated eddy formation to the east off Vietnam affect not only local flow field but also the circulation pattern across the entire SCS. With complex forcing regime and quite limited observation data, our understanding of SCS circulation is still primitive. In particular, the dynamical rationalization of the circulation and its variability in the SCS have not been established.

[3] A number of modeling studies [e.g., *Shaw and Chao*, 1994; *Chu et al.*, 1999; *Metzger and Hurlburt*, 1996, 2001; *Xue et al.*, 2004] have been conducted in the SCS. These studies have greatly improved our understanding of oceanic circulation in the SCS. The findings from the previous modeling studies will be introduced in combination with our analysis. Many previous modeling studies, however, used low horizontal (generally >20 km) and vertical (<30 levels) grid sizes, which may not be large enough to resolve the steep topography and mesoscale flow fields in the SCS and in the Luzon Strait where the KU is located [*Metzger and Hurlburt*, 2001]. In addition, most of previous modeling studies utilized lower frequency atmospheric and lateral fluxes. This would lead to unrealistic representations of forcing and of associated dynamics.

[4] This modeling study investigates the mean seasonal characteristics of the flow field and associated dynamics. An outline of the paper is as follows. The formulation and implementation of the model are described in section 2. Characteristics of three-dimensional circulation and thermal structures as well as comparisons of model outputs with observations are presented in section 3. In section 4, the dynamical balances associated with circulation fields are investigated. Sensitivity studies of the KU intrusion to wind stress and to the NEC are discussed in section 5. The results are summarized in section 6.

## 2. Ocean Model

[5] The ocean model used in this study is the Princeton Ocean Model (POM) [*Blumberg and Mellor*, 1987] for three-dimensional, time-dependent oceanographic flows governed by hydrostatic primitive equations. The *Mellor and Yamada* [1982] level 2.5 turbulent closure scheme is used to parameterize the vertical mixing. The model domain extends from 1.5°N to about 26°N in the north-south direction, and from about 100°E to 130°E in the east-west direction. It includes the region east of the Philippines so that the KU dynamics can be incorporated (Figure 1). A

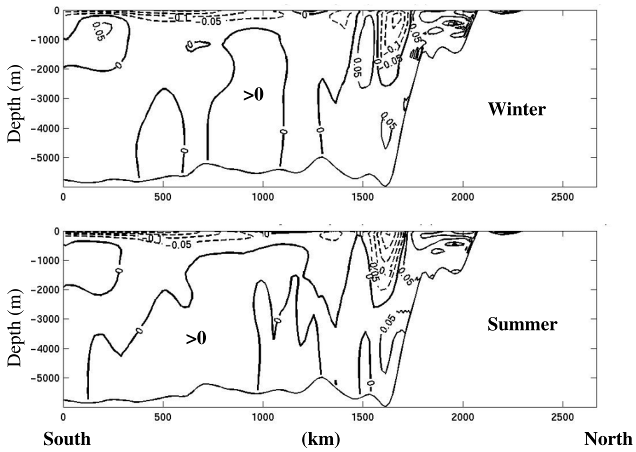


**Figure 2.** Seven-year (1997–2003) average depth-dependent velocities (m $s^{-1}$) normal to the eastern open boundary obtained from the Pacific Ocean Model for the winter and summer, respectively. Among them, the 7-year winter fluxes from the Pacific Ocean model are used during model spin-up. Positive values refer to eastward flows.

curvilinear horizontal grid is utilized with its coordinates $(x, y)$ oriented roughly in the northeast-southwest and the north-west-southeast directions, respectively. The numbers of grid points in the horizontal $(x, y)$ and vertical $(\sigma)$ directions are 259, 181, 30. The horizontal grid spacing is variable, with small spacing ($\Delta x$, $\Delta y$ = about 10 km) in the northern and central parts of the domain and a much larger grid size ($\Delta x$, $\Delta y$ = $\sim$20–30 km) in the eastern and southern parts of the domain. The bottom topography is obtained from ETOPO2 (1/30°) data from the National Geophysical Data Center. The bathymetry is slightly smoothed to reduce truncation errors.

[6] The active open boundary conditions (OBCs), developed by *Gan and Allen* [2005b] and successfully applied in a limited-area modeling study [*Gan et al.*, 2005] are implemented in the eastern and southern open boundaries. Briefly, the OBCs allow disturbances from the interior to propagate freely outward during outflow conditions and the external fluxes to be integrated into the SCS during inflow conditions. The OBCs separate the model variables at the open boundary into global (unforced) and local (forced) parts. The global part of the solution is used in Orlanski-type radiation conditions to determine the character of the boundary solution in regard to the propagation direction of the disturbances. This approach is physically sensible in term of using unforced Orlanski-type radiation OBCs on the forced open boundaries in the SCS. The local parts of eastward and westward depth-integrated velocities ($U$, $V$), depth-dependent velocities ($u$, $v$), temperature ($T$), and salinity ($S$) are obtained from a Pacific Ocean model [*Curchitser et al.*, 2005]. The Pacific Ocean model utilizes ROMS (Regional Ocean Modeling System, *Shchepetkin and McWilliams*, [2005]). The model domain covers the region from 30°S–65°N and 100°E–70°W with a horizontal grid size of 40 and 30 vertical levels. The forcing for the hindcast stage of the simulation in the Pacific Ocean model is derived from the daily National Centers for Environmental Prediction (NCEP, NOAA) Reanalysis data set. After an initial spin-up of 10 years (starting from the Levitus climatology), the Pacific Ocean model was run in hindcast mode for the years 1997–2003 and outputs of every 3-day average are archived to provide lateral fluxes for the SCS model. Figure 2 shows the 7-year mean vertical structures of velocity normal to the eastern open boundary of SCS model domain from the Pacific Ocean model. Westward flows of NEC appear in the upper 200–500 m of water extending northward to about 1100 km from the south. A southward retreating of the NEC occurs in the summer. Much weaker flows are found in the waters deeper than 1000 m. Overall, the flow fields obtained from the Pacific Ocean model have good agreement with the findings from previous studies [e.g., *Qu and Lukas*, 2003].

[7] The SCS ocean model is initialized with the 7-year mean (1997–2003) winter (December–February) temperature ($T$) and salinity ($S$) from the Pacific Ocean model. The model is spun-up for 1500 days forced with the 7-year mean atmospheric wind stress in the winter obtained from the 1 × 1°, 6-hourly NCEP data and with the 7-year mean winter lateral fluxes at the open boundaries obtained from Pacific Ocean model. The 7-year mean surface heat flux is applied during the model spin-up, which is calculated from the bulk aerodynamic formula [*Gan and Allen*, 2005a] using the NCEP meteorological variables of the 6-hourly wind stress at 10 m, the surface air temperature, the relative humidity at 2 m, the cloud cover and the sea level pressure of 1 × 1° resolution. The 6-hourly shortwave radiation is retrieved from NCEP Reanalysis 1 with a 2.5° × 2.5° resolution. In order to avoid uncertainty from using time-mean atmospheric heat flux during model's spin-up, an additional relaxation correction term, similar to the approach adopted by *Gan et al.* [1998] is introduced in the temperature equation during the model spin-up. It takes the form

$$\frac{\partial TD}{\partial t} + \frac{\partial TuD}{\partial x} + \frac{\partial TvD}{\partial y} + \frac{\partial T\omega}{\partial \sigma} = \frac{\partial}{\partial \sigma}\left(\frac{K_H}{D}\frac{\partial T}{\partial \sigma}\right) + F_T + \tau D(T^* - T), \qquad (1)$$

where $D = H + \eta$ ($H$ is bottom topography and $\eta$ is surface elevation), $\omega$ is the vertical velocity in the $\sigma$ coordinates, $K_H$ is the vertical diffusive coefficient, $F_T$ is the horizontal diffusion, $\tau$ is an inverse time constant that takes the value of 1 day at the surface ($\sigma$ = 1) and zero elsewhere, $T^*$ is the input field obtained from the 7-year average MODIS 0.25° × 0.25° sea surface temperature (SST) in the winter. Thus the thermal flux at the surface during model's spin-up is controlled by both the observed SST and the atmospheric heat flux while the solar radiation is allowed to penetrate across the sea surface into the upper ocean. The salinity flux due to evaporation and precipitation is neglected in this study. The time series of the domain average of the kinetic energy (KE) and temperature (Figure 3) shows that the ocean reaches a statistical equilibrium in about 1000 days. The fact that the dynamic and thermodynamic fields in the model are able to reach an equilibrium state also suggests the stable performance of the implemented OBCs. After the 1500 days spin-up, the SST relaxation scheme is turned off. The model is then run the hindcast mode forced with time-dependent atmospheric and lateral fluxes from 1 January 2000 to 30 June 2003. Outputs from 3-year (July 2000 to June 2003) averages

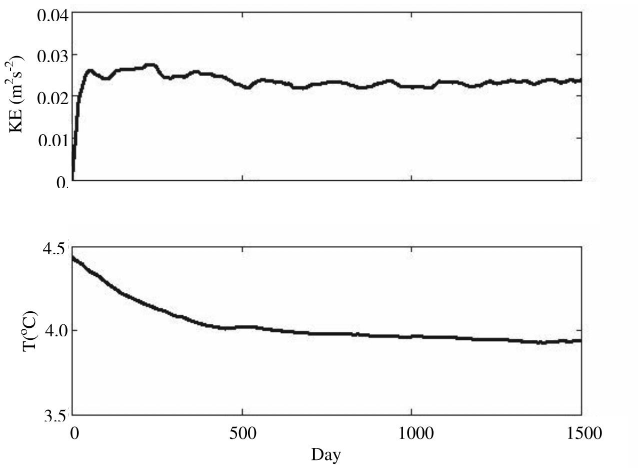


**Figure 3.** Time series of the domain average kinetic energy ($m^2$ $s^{-2}$) and temperature (°C) during model spin-up.

of the winter (December–February), spring (March–May), summer (June–August) and fall (September–November) are used for the analysis.

## 3. Characteristics of the Mean Seasonal Wind Field and SCS Circulation

### 3.1. Monsoonal Wind Stress

[8] Seasonal characteristics of the wind stress fields and corresponding wind curls in the SCS are presented in Figure 4. In the winter, the monsoonal wind stress is directed southwestward over entire SCS and is reversed in the summer. The maximum magnitudes of the wind stress in the winter and summer are approximately located along an axis oriented in a northeast-southwest direction across the central part of the SCS, which form wind curls of the opposite sign on the two sides of the axis. A stronger negative wind stress curl is found in the NSCS and SSCS in the winter and summer, respectively. The winter wind field shifts to a summer one in spring, starting in the SSCS with the onset of the summer monsoon in southern Asia. On the contrary, the transition from the summer to the winter regime in the fall starts in the NSCS. It can be concluded that on the annual average, the winter regime dominates in the NSCS and the summer one in the SSCS. As is shown below, the seasonal upper layer circulation patterns and their transitions in the SCS are highly correlated with the seasonal wind circulation patterns.

### 3.2. Seasonal Circulation

[9] The mean seasonal fields of the surface velocity vectors are shown in Figure 5a and the fields of velocity vectors averaged over the upper 200 m water and at depths of 500 m and 2000 m are shown in Figure 5b. The relative vorticity, ($\zeta$), divided by the Coriolis parameter ($f$) are presented in Figure 6. In response to the wind-forcing, basin-wide cyclonic and anticyclonic general circulations are formed in the upper layer during the winter and summer, respectively. These circulation patterns are characterized by the strong currents along the continental margin in the northern and western SCS. The existence of eddies embedded within the general circulation is also evident. In winter, two cyclonic eddies labeled as $W_1$ and $W_2$ are located to the west off the northern Philippines and to the east off southern Vietnam, respectively. The eddy $W_1$ is formed by the southwestward currents near the continental slope and the northward currents west of the northern Philippines, and extended vertically to about 200 m. The eddy $W_2$ existed in the water depth of upper 200 m, is formed as southward currents moving along the continental margin on the western part of the SCS and separate near promontory of the coast at about 12°N and subsequently follow the bottom isobath along the shelf margin. The circulation associated with $W_1$ dominates the flow pattern in the NSCS while the circulation associated with $W_2$ regulates the flow field in the SSCS in the winter. Relatively weak southwestward alongshore currents are found over the continental shelf in the NSCS. This can be partly ascribed to the existence of a negative wind curl in the region and to the shelf topography not being well resolved by the model. In the summer, circulation pattern is reversed in response to the summer monsoon. A cyclonic eddy ($S_1$) and an anticyclonic eddy ($S_2$) appear southeast of Hainan. It appears that the strength of $S_1$ is weaker as compared with

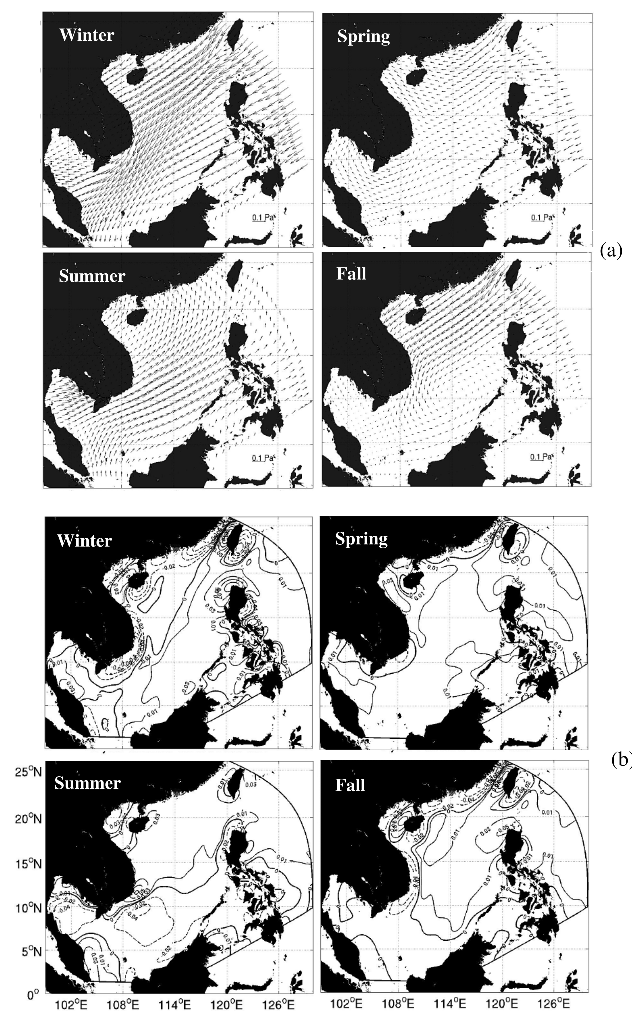


**Figure 4.** Three-year (July 2000 to June 2003) seasonal mean (a) wind stress vectors and (b) wind stress curls calculated from NCEP 1 × 1° Reanalysis data.

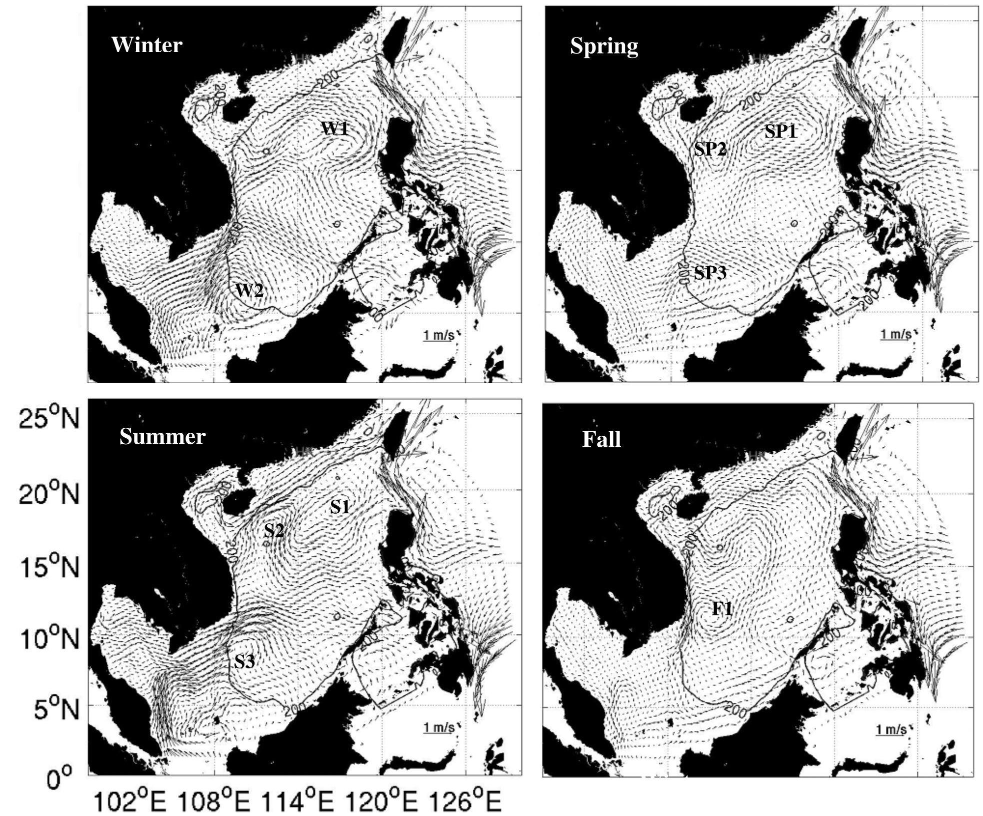


**Figure 5a.** Mean seasonal surface velocity vectors (m $s^{-1}$). Major eddies embedded in the circulation are also marked.

$W_1$ at the approximately same location in the winter. On the contrary, the intensity of $S_2$ is stronger than the corresponding one in the winter. The anticyclonic eddy ($S_3$) located to the east off southern Vietnam, is a recirculation formed by the separation of the northeastward coastal current, which is mainly response to wind stress of a dipole structure in the region as shown in Figure 4. Over the shelf in the NSCS, the direction of the mean wind stress is southerly in the summer. Hence the part of northeastward alongshore currents over the NSCS region east of Hainan Island is likely contributed by the inflows along the continental margin southwest of Hainan. The winter-summer-winter transitions of circulation occur in the spring and fall following the transitions in the wind field. In the spring, the circulation is shifting from winter regime to summer one starting from the SSCS while it is returning into the winter regime starting from the NSCS in the fall. The circulation patterns described above and existence of eddies in the SCS during winter and summer are very similar to the observations by *Wyrtki* [1961], *Xu et al.* [1982], and *Qu et al.* [2000] based on historical hydrography data. They are also in good agreement with the results derived from remote sensing data as will be shown.

[10] East of the Philippines, the flow field is dominated by the KU in all seasons (Figures 5a and 5b). The KU is seen to overshoot into the Luzon Strait from the northern tip of the Philippines Islands, turns northeastward north of the Luzon Strait and moves along the east coast of Taiwan toward the Pacific. Part of the KU, however, continues flowing northwestward north of the Luzon Strait without turning northeastward. This component of the KU typically turns southwestward at the edge of the shelf southwest of the Taiwan and intrudes into the SCS along the continental margin. The intrusion of the KU in the upper layer occurs in the winter, spring and fall as shown in Figure 5a. Similar circulation patterns are also found in the velocity fields averaged over upper 200 m. However, much weaker strengths of the circulation and of the eddies $W_1$, $W_2$, $S_1$ and $S_3$ in the upper 200 m average field imply the dominant role of wind forcing in the upper layer circulation. Weaker depth-dependent flow is, however, detected in the upper 200 m in the KU. An anticyclonic eddy is found south of Xisha at depth 500 m in the winter and summer, reflecting the effect of local bottom topography on the flow field. The KU intrusion in deep water is also evident in the velocity field at 2000 m, but not at 500 m, forming an alternate flow pattern of inflow-outflow-inflow in the surface-intermediate-deep layers in the Luzon Strait, respectively. More details about the depth-dependent circulation are presented in section 4.

[11] The strength of the surface flows and the associated eddies can be measured by the field of surface relative vorticity ($\zeta$) divided by $f$ (Figure 6). Large values are found to be associated with the eddies and strong currents across the SCS. The major eddies existed in the different seasons are indicated by positive and negative values for cyclonic and anticyclonic eddies, respectively. The strongest eddies

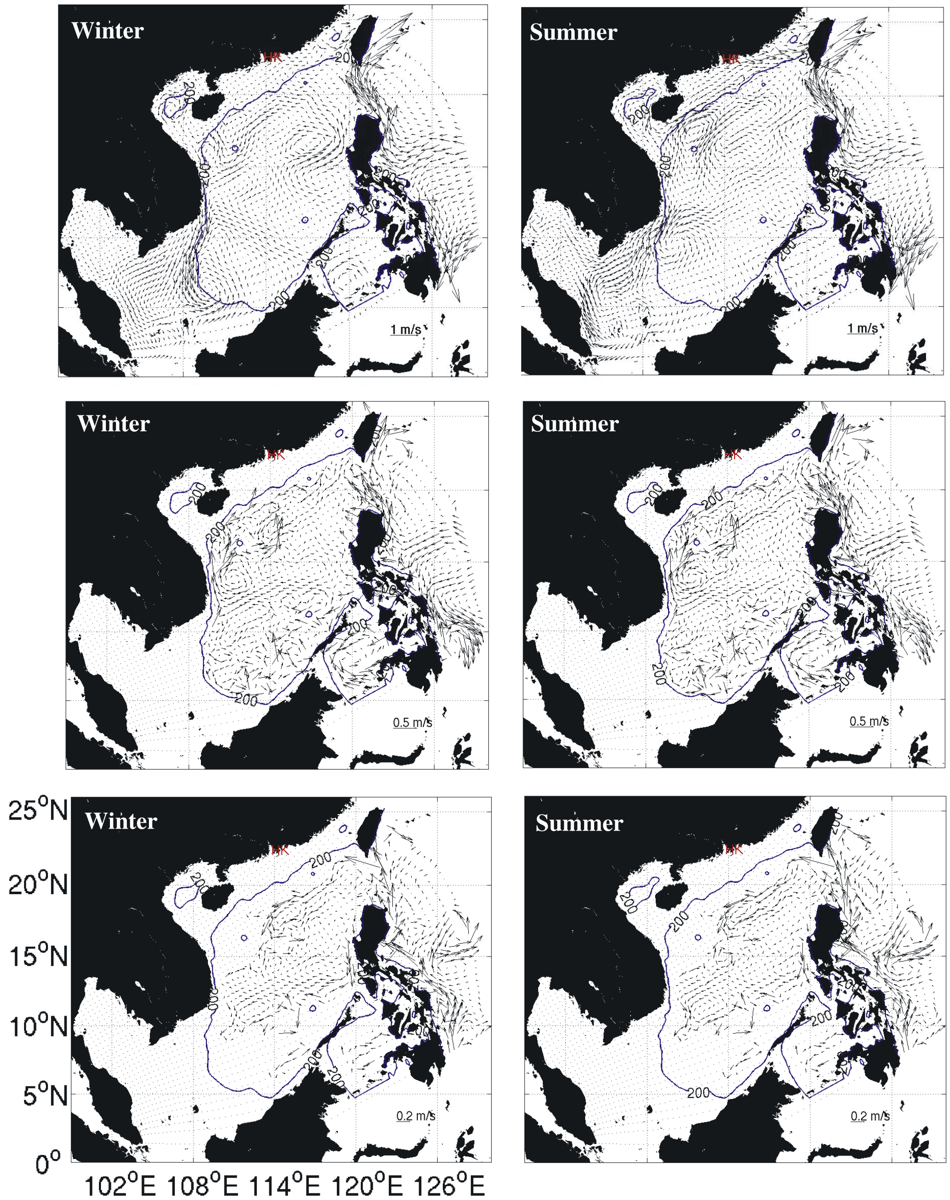


**Figure 5b.** Mean velocity vectors (m s$^{-1}$) averaged (top) in the upper 200 m and at the depths of (middle) 500 m and (bottom) 2000 m for the winter and summer.

are those caused by the coastal current separation off Vietnam in the SSCS. The vorticity along KU shows a jet-like feature with the opposite sign of $\zeta/f$ located on the western and eastern sides of the jet core. Larger values are found in the winter and spring, indicating a stronger horizontal shear in the KU. In particular, the existence of a large positive vorticity west of jet core on the northern part of the Luzon Strait in the winter and spring could provide a favorable condition for the KU to veer westward into the SCS. This positive vorticity is markedly weakened in the summer and fall.

### 3.3. Model-Observation Comparisons

[12] Observation data from the SCS is very limited, particularly in regard to the velocity fields. Data obtained from satellite remote sensing has been used for qualitative extraction of circulation characteristics. The simulated and observation-derived mean circulation and thermal fields in the winter and summer are selected to conduct model-observation comparisons here.

[13] The weekly altimetry data from TOPEX/POSEIDON (T/P) is used to calculate the surface geostrophic current by the surface geopotential height, $H_g$ [*Li et al.*, 2003]:

$$H_g = \overline{H_g} + gh_g, \tag{2}$$

where $\overline{H}_g$ is time mean value and is estimated from $1^\circ \times 1^\circ$ gridded climatological temperature and salinity data [*Levitus and Bayer*, 1994a, 1994b], $g$ is the gravity acceleration and $h_g$

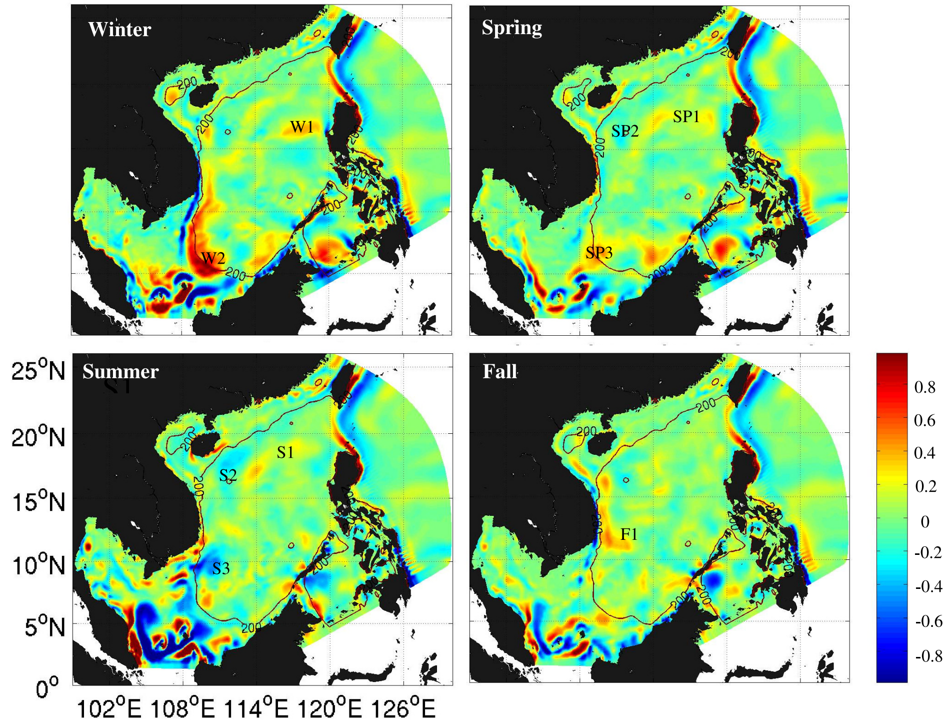


**Figure 6.** Same as Figure 5a, but for the field of mean seasonal surface vorticity, ξ, divided by the Coriolis parameter, *f*.

is the sea surface height anomaly (SSHA) obtained from T/P data. After obtaining the surface geopotential height, geostrophic current can be retrieved according to the geostrophic balance. Results from SSHA in water shallower than 200 m and around islands may be contaminated and caution is advised in assessing the outcome. Geostrophic velocity from the model is obtained by the pressure gradient and the Coriolis force terms (equations (3) and (4) in section 3.4).

[14] The mean seasonal surface geostrophic velocity vectors as well as $h_g$ obtained from both the model and T/P data for the winter and summer are shown in Figure 7a. A qualitatively similar basin-wide circulation pattern is found in the velocity fields derived from model and observation. In particular, the horizontal scales and the locations of eddies $W_1$ and $W_2$ in the winter are well matched in both fields. Similar conditions occur in the summer with well-simulated coastal current separation and the recirculation $S_3$. In the north, the simulated cyclonic $S_1$ and anticyclonic $S_2$ are also detected in the T/P-derived velocity field. The $S_1$ and $S_2$ from modeling result, however, are located farther west compared with velocity field derived from observation. Both velocity fields show that the mainstream of the KU separates from the northern tip of the Philippine Islands, passes through the Luzon Strait and flows eastward along the eastern coast of Taiwan in the winter and summer. In addition, both the model- and T/P-derived surface geostrophic currents indicate the possible westward intrusion of the surface KU into the SCS in the winter and the northeastward turning of the surface KU without the intrusion in the summer. Additional evidence supporting the simulated KU path in the Luzon Strait can be seen from the winter satellite SST data (Figure 7c) in the KU which shows a track of warm surface water being advected northward across the Luzon Strait. Overall, the simulated velocity is qualitatively similar to the field derived from the T/P data. Stronger values found in the simulated velocity may be ascribed to many reasons like the unrealistic representation of climatological density field used in (2), smoothed observational estimates and others. Regarding this issue, direct comparison of SSHA fields is conducted. The simulated $H_g$ is calculated by subtracting the 3-year mean SSH obtained from the model. Figure 7b shows that simulated and observed SSHA well resemble each other. They both show the negative/positive SSHA centers to the west of Philippines and to the east off southern Vietnam in the winter/summer, corresponding to the seasonal flow fields in these locations. In addition, positive and negative values of SSHA in the coastal waters over the northern and western shelves and in the Gulf of Thailand are found in both fields in the winter and summer, respectively. The findings suggest that the model is able to realistically capture the dynamic conditions in the SCS. Comparison of the SST fields obtained from the model and MODIS also show a good agreement (Figure 7c). In winter, both results indicate the existence of cold waters over the NSCS, which extends southwestward and subsequently southward along the continental margin to the western part of the SSCS. Warmer SST, however, is shown in the simulated field in the NSCS. High SST is found in the Gulf of Thailand and in the coastal region southeast of the basin in both simulated and observed fields. The KU is indicated by the

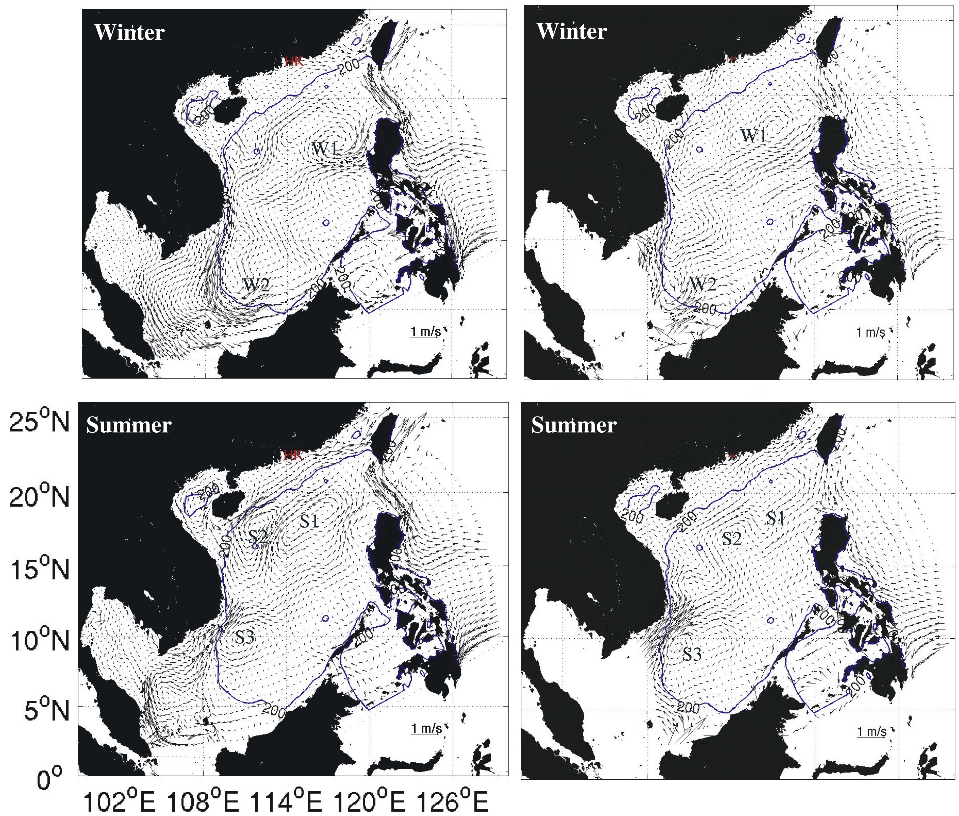


**Figure 7a.** Mean surface geostrophic velocity vectors (m s$^{-1}$) from (left) model and (right) derived from altimetry data in the winter and summer.

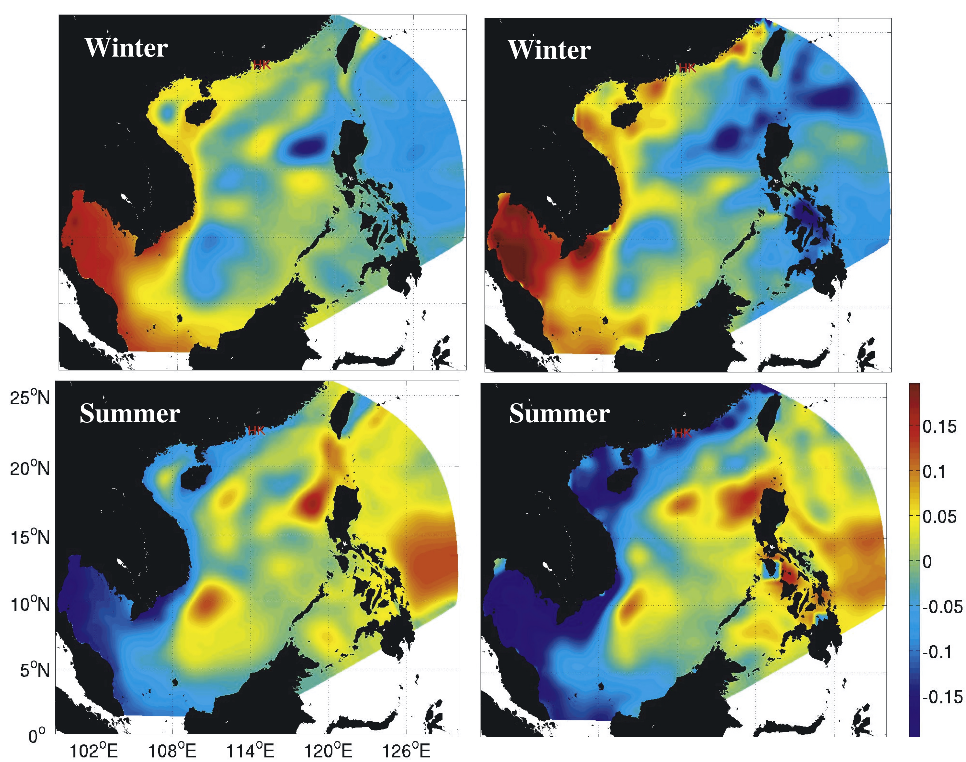


**Figure 7b.** Mean sea surface height anomalies (SSHA, m) from the (left) model and (right) derived from T/P altimetry data in the winter and summer. Additional 0.05 m is subtracted from the T/P data.

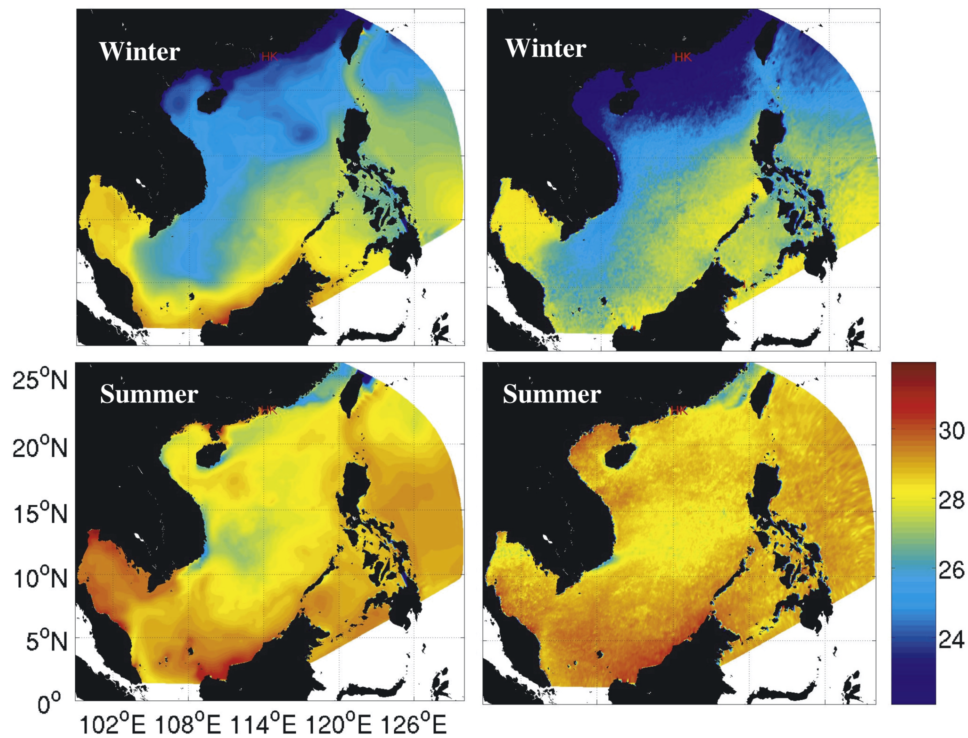


**Figure 7c.** Mean winter and summer sea surface temperatures (°C) from the (left) model and (right) MODIS data, for the winter and summer.

warmer water track in the Luzon Strait in both observed and simulated fields. Other resemble SST features between the simulation and observation in the summer include warm surface waters of about 29°C in the entire SCS and colder waters in the regions of the Taiwan Strait, to the southeast of Hainan and to the east off Vietnam. The results from both model and observation also show that cold waters originated from the coastal upwelling to the east off Vietnam [*Xie et al.*, 2003] in summer can penetrate into the interior of the SCS. Although the SST features between the simulated and observed fields are qualitatively similar, the quantitative difference exists between the two fields, particularly over the shelf region where a model with a smaller grid size may be required to more accurately resolve the shelf topography.

[15] In order to further conduct qualitative comparison of the seasonal circulation features in the SCS and in the KU, the 20-year (1984–2003) mean surface drifter tracks from MEDs/GTS (Marine Environmental Data Service/Global Telecommunications System, Canada) are shown in Figure 7d. The field of the drifter tracks in the winter suggest that a basin-wide cyclonic circulation pattern in the SCS is formed by currents along the continental margin of the SCS. Especially, drifters in the Pacific Ocean are likely to flow into the SCS by the KU in the winter

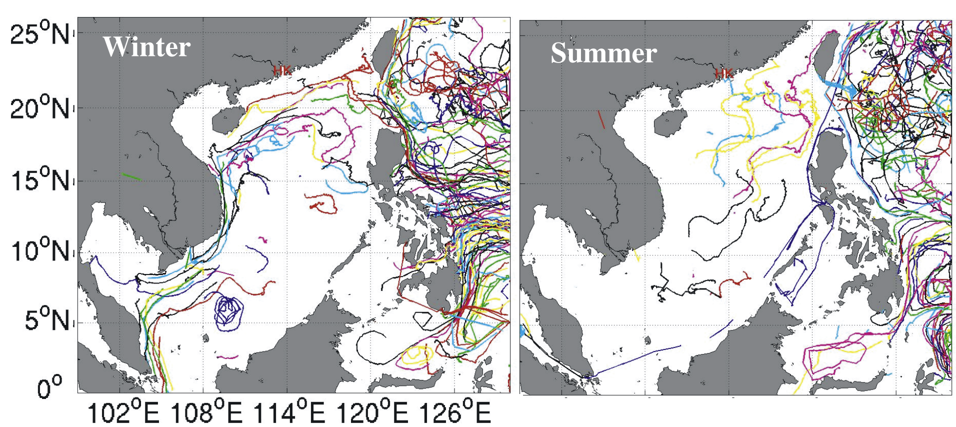


**Figure 7d.** The 20-year (1984–2003) surface drifter tracks for the (left) winter and (right) summer.

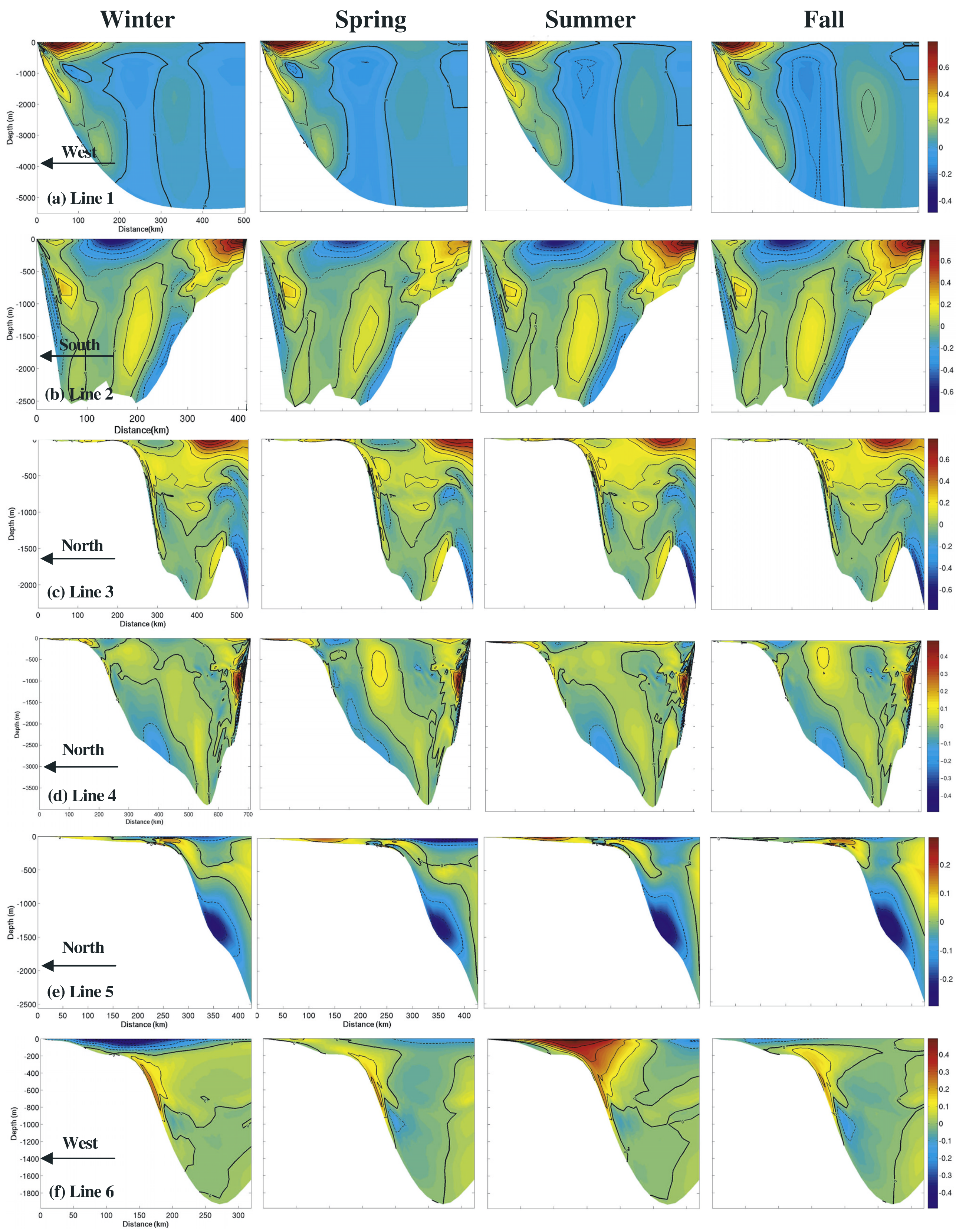


**Figure 8.** Mean seasonal cross sections of velocity (m s$^{-1}$) normal to lines 1, 2, 3, 4, 5, and 6 as shown in Figure 1. Positive (solid contours) values refer to the velocities directed to the northwestward for line 1, to eastward for line 2, and to northeastward for lines 3–6, respectively. The contour interval for velocity is 0.1 m s$^{-1}$ with a heavy contour line for a zero value.

and not in the summer. This is consistent with the model results of upper layer circulation. East of the Philippines, the drifter tracks indicate that the NEC bifurcation occurs at about 15N in the winter but shifts southward in the summer.

[16] Overall, the above comparisons show the similarities between simulated and observation, which establishes a level of confidence in the model.

### 3.4. Vertical Structure in Flow Field

[17] Vertical structures of the circulation in the SCS are illustrated by the cross sections (Figure 1) of velocity around the basin (Figure 8). In the section east of the Philippines (line 1, Figure 8a), the mainstream of KU is found within 200 km from the coast with a maximum speed of about 1 m s$^{-1}$ at the surface and with little seasonal variation. It extends vertically to about 500 m, with additional branch extending to more than 4000 m over the slope. At 250 km offshore, a southward current is centered at a water depth of 1000 m and extended to the bottom, showing a strong barotropic character. As the KU moves northward, it directs northwestward south of the Luzon Strait as shown in Figure 5a. The vertical structure of the velocity in the Luzon Strait (Figure 8b) can be seen by the cross section of velocity normal to line 2. The core of westward KU locates in the upper 500 m water between 100 and 300 km from the south shore and shifts slightly southward in the summer and fall. The eastward currents north of the Luzon Strait have a width about 100 km and reach vertically to 1000 m. Westward inflows are also found in the deep water over the southern and northern slopes, and beneath the core of westward KU in the upper layer. The cross section of thermal fields (not shown) in lines 1 and 2 indicate that the thermocline is generally shallower in the near-coastal region in response to the local currents.

[18] The cross sections of the velocity from line 3 to line 6 (Figures 8c–8f) illustrate the vertical flow structures of seasonal circulations around the SCS. In particular, since the KU may loop out near Luzon Strait without intruding into the SCS, cross sections of velocities along lines 3 and 4 can be used to identify the condition of possible westward intrusion of the KU. At line 3 (Figure 8c), the intrusion of the KU occurs near the shelf break with a southwestward (normal to line 3) current in the upper 200 m in the winter, spring and fall, similar to the finding shown in Figure 5a. The southwestward intrusive currents also exist in the northern slope below 1000 m in all seasons. At the cross section of line 4 (Figure 8d) located farther west of line 3 (Figure 1), the westward currents are also found in the upper 200 m near the shelf break and below 1000 m over the northern slope. Combined with similar westward flows in line 3, it suggests that the KU does intrude into the SCS in the upper 200 m near the shelf break and below 1000 m over the northern slope. Another branch of intrusion at line 4 is found south of central section extending from surface to the bottom in the winter and spring and from 500 m to more than 2000 m in the summer and fall. This branch of the westward current is likely associated with the component of northwestward flowing KU in the central part of the Luzon Strait as indicated in Figures 5b and 8b. It is also clear that the westward currents over the southern slope of the Luzon Strait in Figure 8b do not penetrate into the SCS locally since they have not been seen in the south shore of line 4. These results, together with the flow fields at depths in Figure 5b, clearly demonstrate the existence of the KU intrusion in the upper layer mainly in winter, spring and fall and at depths in all seasons. *Qu et al.* [2000] also found a KU intrusion into the SCS all year-round at the continental slope south of China. *Shaw* [1991] and *Shaw and Chao* [1994] showed that intrusion of the KU is less likely to occur in the summer, but suggested the possible existence of an intrusion path along the continental slope.

[19] The cross section of velocity at line 5 (Figure 8e) reflects the seasonal circulations in the central region of the NSCS. Over the inner shelf, southwestward currents occur in the winter and fall while northeastward currents exist in the summer and spring. There also exists a southwestward current in the upper 200 m extending from 200 km (water depth 200 m) to about 400 km (water depth 2500 m) offshore in all seasons. This current can be seen in Figure 5a of the upper layer circulation and is mainly associated with the local cyclonic eddies. Similar to the conditions in lines 3 and 4, the southwestward currents are found at depths over the continental slope in all seasons in line 5. With deep circulation shown in Figure 5b, it is evident that these southwestward currents is likely originated from the KU intrusion. Vertical structures of seasonal flow in the region to the east of Vietnam are shown in the cross section of velocity normal to line 6 (Figure 8f). The southwestward coastal currents in the upper 200 m with an offshore extension of about 300 km occur in the winter, while the northeastward coastal currents in the upper 800 m with smaller horizontal extension (about 200 km) exist in the summer. Their transition modes are displayed in the spring and fall.

[20] The cross sections of temperature at lines 3–6 (not shown) are mainly in response to the flow fields. In particular, a deepening of the thermocline is found near the shelf break at lines 3–4 in association with the intrusive component of the KU in the upper layer. Upward and downward tilting of isotherms in the coastal regions at lines 5 and 6 are typically induced by the coastal upwelling in the summer and downwelling in the winter, respectively. The cross sections of velocity and temperature at lines around the SCS further illustrate the circulation patterns presented in sections 3.2 and 3.3 and reveal the characteristics of KU intrusion. In particular, it demonstrates the vertical structures of the flow in the SCS as well as in the KU.

## 4. Dynamics of Circulation

[21] To help identify the dynamical processes that control the circulation in the SCS, momentum balances are exam-

**Figure 9a.** Upper 200 m average fields of Coriolis force (COR), pressure gradient (PRE), ageostrophic pressure gradient (AGE), nonlinear advection (NL), and vertical diffusion (DIFF) terms in the momentum equation (1) divided by water depth (in m s$^{-2}$, multiplied by $10^5$ for COR and PRE and by $10^6$ for NL, AGE and DIFF) for (left) winter and (right) summer. The results are rotated to zonal ($x'$, east-west) axis.

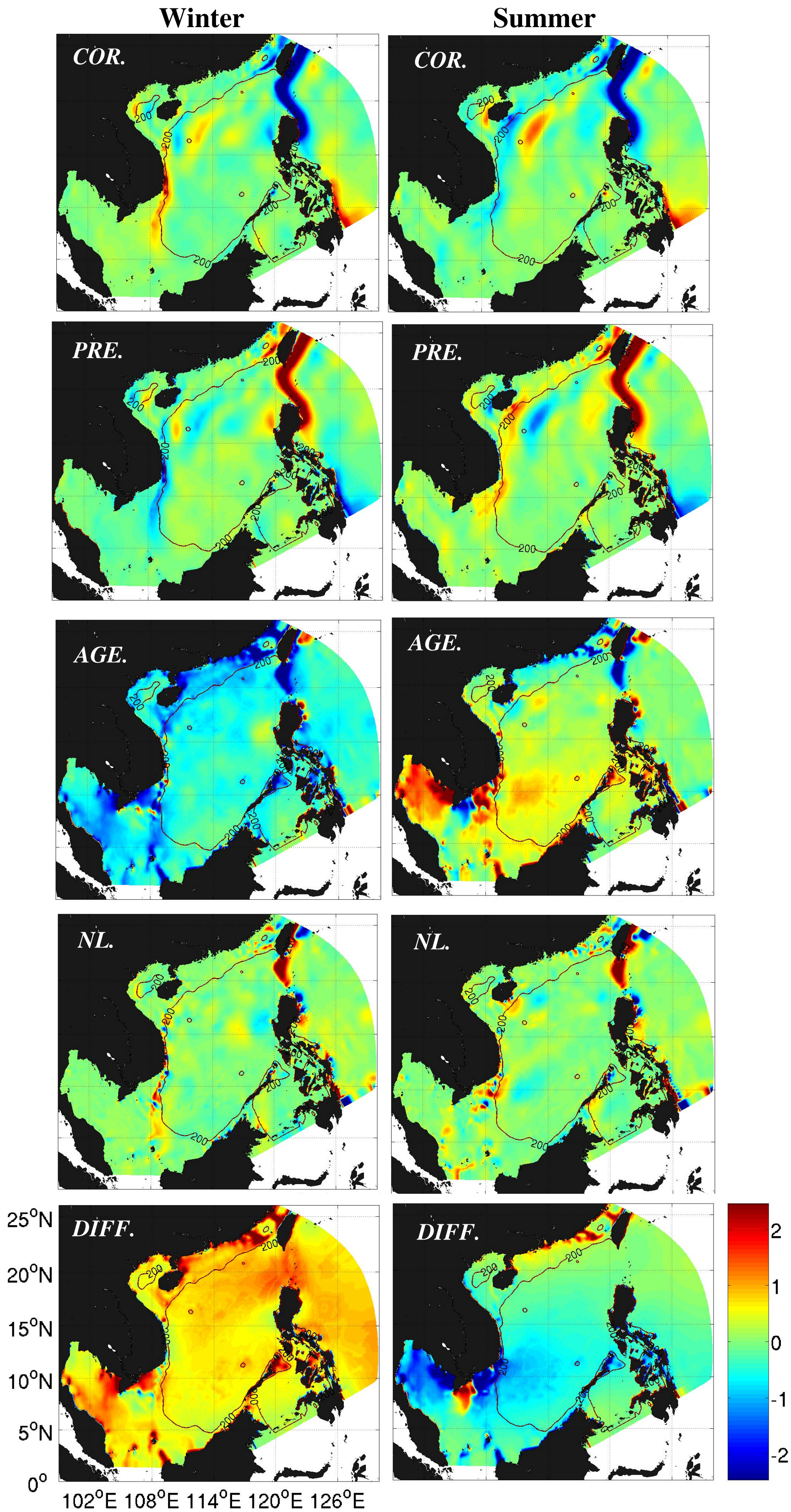
Winter
Summer
COR.
PRE.
AGE.
NL.
DIFF.
200
25°N
20°N
15°N
10°N
5°N
0°
102°E 108°E 114°E 120°E 126°E
2
1
0
-1
-2

**Figure 9a**

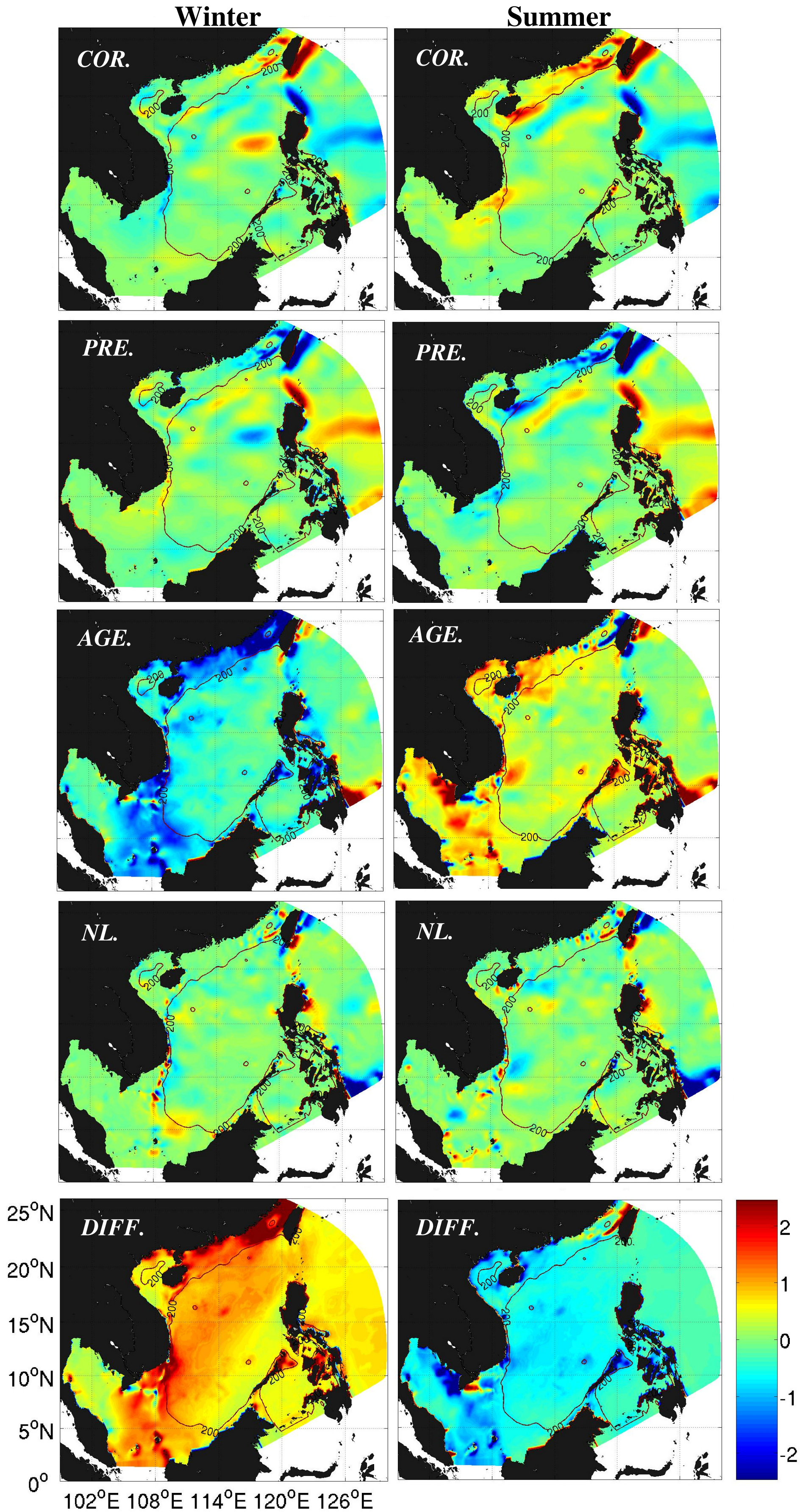


**Figure 9b.** Same as Figure 9a, but for longitudinal ($y'$, north-south) axis.

ined. The conditions in the winter and summer are selected to illustrate the seasonal characteristics of the momentum balance in the SCS.

### 4.1. Momentum Equations

[22] The depth-dependent momentum equations for $(x, y)$ are given in equations (3) and (4), respectively.

$$\overbrace{\frac{\partial uD}{\partial t}}^{1} + \overbrace{\frac{\partial u^2D}{\partial x} + \frac{\partial uvD}{\partial y} + \frac{\partial u\omega}{\partial \sigma} - F_x}^{2} - \overbrace{fvD}^{3} - \overbrace{\frac{\partial}{\partial \sigma}\left(\frac{K_M}{D}\frac{\partial u}{\partial \sigma}\right)}^{4}$$
$$\overbrace{+gD\frac{\partial \eta}{\partial x} + \frac{gD^2}{\rho_0}\int_\sigma^0 \left(D\frac{\partial \rho'}{\partial x} - \frac{\sigma'}{D}\frac{\partial D}{\partial x}\frac{\partial \rho'}{\partial \sigma'}\right)d\sigma'}^{5} = 0, \tag{3}$$

$$\overbrace{\frac{\partial vD}{\partial t}}^{1} + \overbrace{\frac{\partial uvD}{\partial x} + \frac{\partial v^2D}{\partial y} + \frac{\partial v\omega}{\partial \sigma} - F_y}^{2} + \overbrace{fuD}^{3} - \overbrace{\frac{\partial}{\partial \sigma}\left(\frac{K_M}{D}\frac{\partial v}{\partial \sigma}\right)}^{4}$$
$$\overbrace{+gD\frac{\partial \eta}{\partial y} + \frac{gD^2}{\rho_0}\int_\sigma^0 \left(D\frac{\partial \rho'}{\partial y} - \frac{\sigma'}{D}\frac{\partial D}{\partial y}\frac{\partial \rho'}{\partial \sigma'}\right)d\sigma'}^{5} = 0, \tag{4}$$

where $F_y$ and $F_x$ are the corresponding horizontal viscosity terms [*Blumberg and Mellor*, 1987], $\omega$ is a velocity normal to $\sigma$ surfaces, and $K_M$ is the vertical turbulent viscosity coefficient; $\rho$ and $\rho_o$ are the water density and reference density, respectively. The notation for other variables is the same as defined in sections 2 and 3.

[23] Since stronger circulation mainly occurs in the upper ocean as shown in sections 2 and 3, terms in (3) and (4) are averaged over the upper 200 m. In addition, the horizontal coordinates $(x, y)$ are rotated to be directed toward the true east and north for $(x', y')$ when horizontal momentum distribution is presented (Figures 9a and 9b). In the cross sections, a component of terms normal to the cross section is presented (Figures 10 and 11). Terms in (3) and (4) are also normalized by water depth $H$ and are referred to as acceleration (term 1), nonlinear advection, NL (term 2), Coriolis force, COR (term 3), vertical diffusion, DIFF (term 4), and the pressure gradient, PRE (term 5). It is also convenient to consider the behavior of the sum of the Coriolis force term 3 and pressure gradient term 5, which is referred to as ageostrophic pressure gradient, AGE.

### 4.2. Dynamic Response to Wind and Kuroshio Forcing

[24] Horizontal $(x', y')$ field of terms averaged in the upper 200 m are plotted in Figures 9a and 9b for the winter and summer, respectively. Momentum balances in both the $x'$ and $y'$ directions are generally dominant by the geostrophic balance in both seasons. In the zonal ($x'$, east-west) direction (Figure 9a), the KU is clearly represented by a large value of negative COR, which is mainly balanced by a positive PRE. Large values of COR and PRE are also found in the coast waters to the east off southern Vietnam along 200 m isobath. The AGE is generally small except in the northern part of the Luzon Strait and in the region to the east off southern Vietnam. A large value of negative AGE is found in the KU at the northern part of the Luzon Strait, provided by the net contribution of local negative COR. Similar pattern and magnitude in the positive value of NL at the same location suggest that this negative AGE is balanced by the positive NL. Clearly, a centripetal acceleration associated with the inertia in the northern part of the Luzon Strait is responsible for the KU's eastward turning. The situation can be illustrated by a horizontal momentum equation along a streamline of the KU,

$$\frac{V_k^2}{R} + fV_k + \frac{1}{\rho_o}\frac{\partial P}{\partial n} = 0, \tag{5}$$

where $V_k$ is the horizontal speed along the KU; $n$ is normal to the streamlines in the KU and is positive to the left of the flow direction. $R$ is the local radius of curvature of the streamline along the KU and is taken to be positive when the center of curvature is in the positive $n$ direction. $P$ is the water pressure. From the results shown in Figure 9a, it is clear that $1/\rho_o\ \partial P/\partial n < 0$, $fV_k > 0$ and $(AGE)_k = 1/\rho_o\ \partial P/\partial n + fV_k > 0$ in the northern part of the Luzon Strait. Thus centripetal acceleration due to the curvature of the KU trajectory $V_k^2/R < 0$ or $R < 0$ suggests that the water parcel in the KU turns toward east following the motion. In the region to the east off southern Vietnam where a coastal jet separation and eddy formation occur, relatively large negative and positive values of AGE in the zonal momentum equation are found in the winter and summer. It appears that large portion of AGE in the region is balanced by NL in the winter and by DIFF in the summer.

[25] The momentum balances in the longitudinal ($y'$, north-south) direction are shown in Figure 9b. Negative and positive values of COR, representing the westward and eastward currents, exist at the southern and northern parts of Luzon Strait, respectively. They are mainly balanced by PRE. Combined with the condition in $x'$, this balance demonstrates that the KU moves geostrophically northwestward from south of the Luzon Strait, turns eastward by the existence of intensified nonlinearity in the zonal direction north of the Luzon Strait, and forms a northeastward geostrophic current along the east coast of Taiwan. In addition, dominant geostrophic balances in $y'$ are found along the continental margin in the NSCS. In the summer, a positive PRE locates over the continental slope in the central part of the NSCS in association with the southwestward current in the local eddy $S_1$ (Figure 5a). In the winter, a similar positive PRE is found over the slope in the location of $W_1$ but extended eastward to the southwest of Taiwan, which could be geostrophically favorable to the KU intrusion in the region. Inertia effect of KU in the Luzon Strait is also indicated by a larger value of NL. Similar to the condition in $x'$ direction, there exist negative and positive AGE to the east off southern Vietnam in the winter and summer, respectively, which are balanced by NL and/or DIFF in the region. Overall, in the coastal jet to the southeast off Vietnam, the wind effect as represented by DIFF is stronger along $x'$ in the summer and along $y'$ in the winter as expected from the wind stress fields (Figure 4). These results suggest that eastward ($x'$) overshooting of the coastal jet (Figure 5a) near the promontory off Vietnam coast in the summer is likely associated with the forcing in the local wind stress field while the separation of the wind-

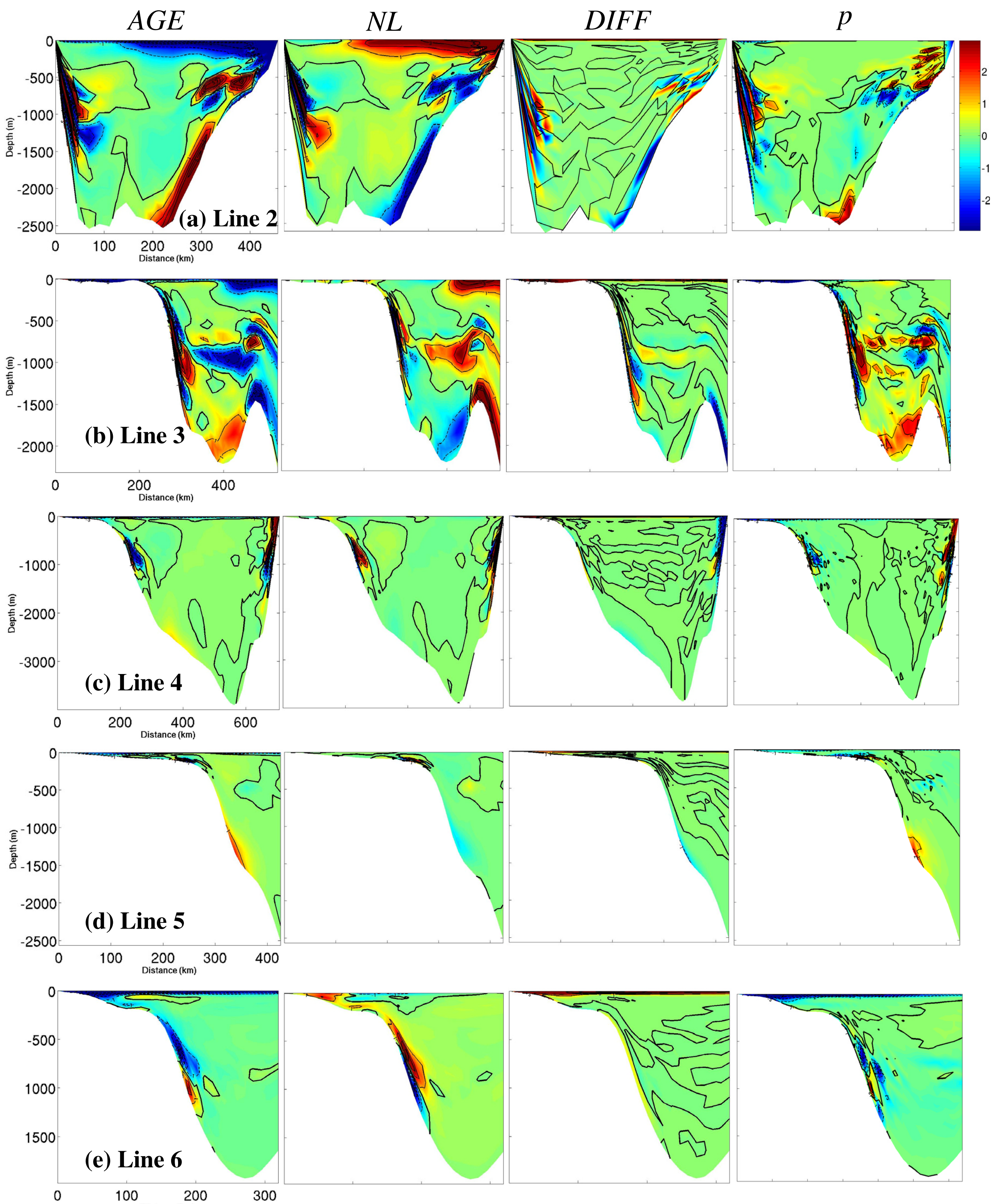


**Figure 10.** Winter values of the ageostrophic pressure gradient (AGE), nonlinear advection (NL), vertical diffusion (DIFF), and net pressure gradient (p) terms in the momentum equation at lines 2–6. Values are rotated to the coordinates normal to the each individual cross section and are divided by water depth (in m s$^{-2}$, multiplied by $10^6$).

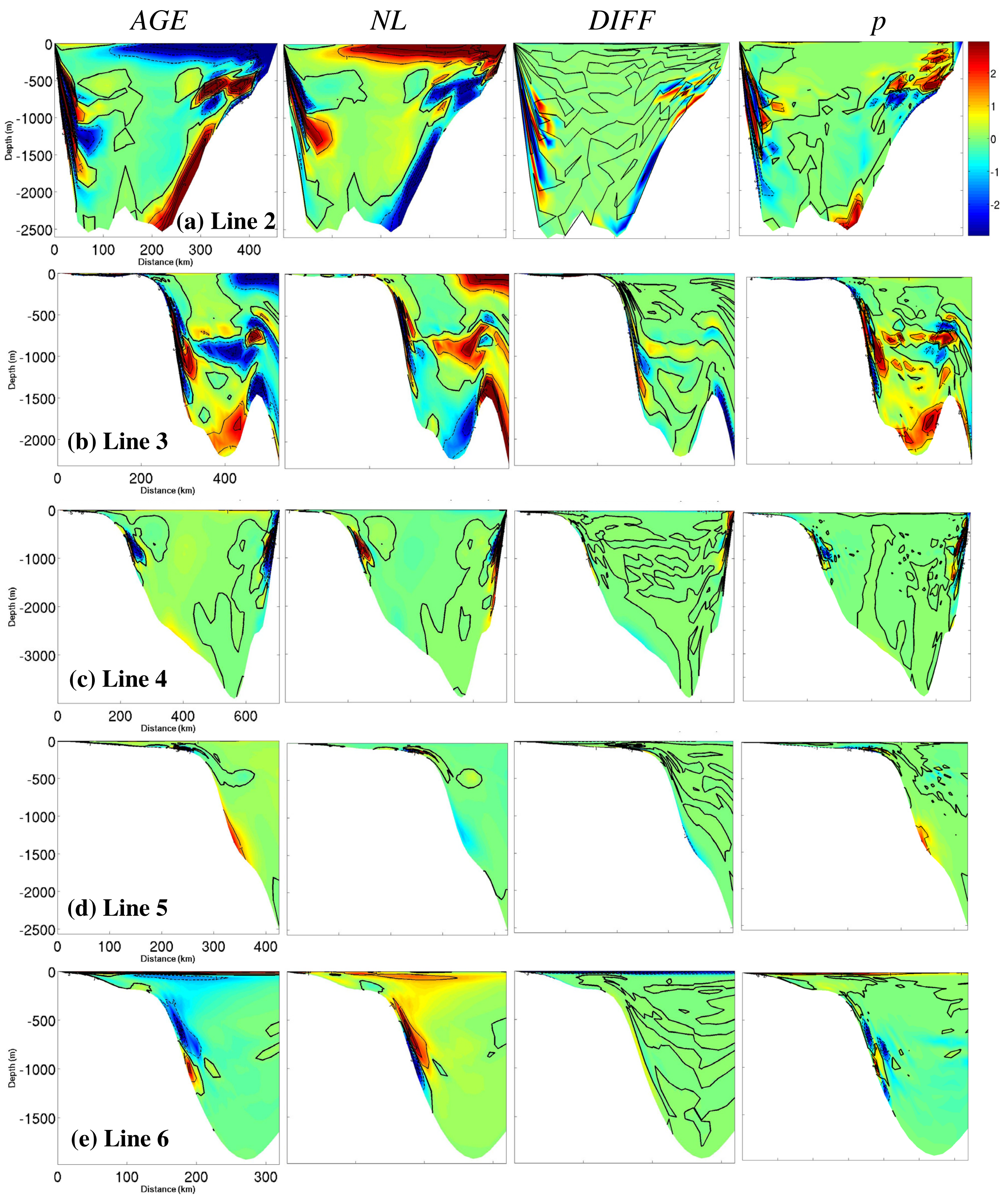


**Figure 11.** Same as Figure 10, but for the summer.

intensified jet along the edge of shelf in the winter is through the jet-shelf topography interaction.

[26] The vertical structure of dynamic balance is obtained by examination of depth-dependent dynamical term balances normal to the cross sections at lines 2–6. In order to obtain the net contribution to AGE from pressure gradient force, which is referred to as $p$, a method described by *Gan and Allen* [2005a] is adopted. The approach removes the common part of opposite sign in PRE and COR that cancels in their sum AGE, and subsequently extracts $p$ from AGE. The terms in (3) of AGE, NL, DIFF and $p$ at lines 2–6 are shown in Figures 10 and 11 for the winter and summer,

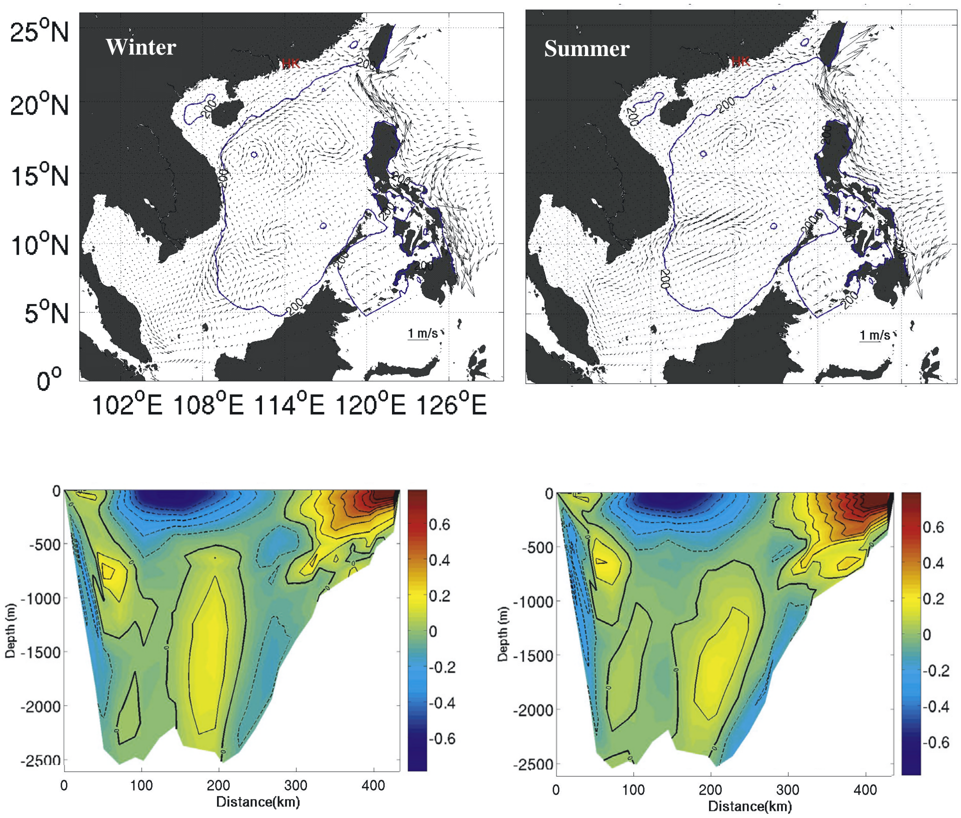


**Figure 12.** Mean velocity vectors (m s$^{-1}$) averaged in the upper 200 m and mean velocity (m s$^{-1}$, positive values refer to eastward flows) normal to the cross section at the Luzon Strait for the case forced with the weakening monsoonal wind stress in (left) winter and (right) summer, respectively.

respectively. At line 2 across the Luzon Strait, positive NL similar to that north of the Luzon Strait in Figure 9a are found in the upper 200 m in both seasons. Opposite sign of NL is found over the northern slope mainly below 1000 m and in the region below 500 m between 100 and 200 km from the south shore, which closely match with the respective westward flows in the same locations (Figure 8b). Similarly, negative values of NL (Figures 10 and 11) and corresponding southwestward currents (Figure 8) in all seasons are found over the northern slope below 1000 m at the cross sections at lines 3, 4, and 5. These negative NL at depths are balanced by the positive AGE which are primarily contributed by net westward pressure gradient force *p*. Thus the results suggest that the westward intrusion of the KU at depths is via ageostrophic currents and is associated with the net westward pressure gradient force. *Qu et al.* [2006], using hydrographic data, also found that below about 1500 m, there is a persistent baroclinic pressure gradient arising from the density difference between Pacific and South China Sea which drives flow westward through the Luzon Strait. In addition, transient eddies and other processes cross the Luzon Strait could also alter local dynamic field and lead to the intrusion of the KU in the deep water. The linkage between the westward intrusive currents and the *p* in the upper layer is, however, not obvious at lines 2–5. In the region to the east off Vietnam coast (line 6), a large value of negative AGE in the inner shelf is balanced by the NL in the winter while a small value of positive AGE is found at the same location in the summer. Relatively large value and deeper penetration of positive NL are found over the midshelf and slope in the summer, corresponding to the similar flow field shown in Figure 8f. Over the slope, negative *p* presumably accelerates the northeastward currents at water depths between 400 and 1000 m indicated in Figure 8f. The northeastward and southwestward *p* are found near surface waters in the inner shelf during the winter and the summer respectively, which could provide an "inverse pressure gradient force" for the coastal jet to separate from the coast [*Gan et al.*, 1997].

## 5. Sensitivity of the Kuroshio Intrusion to Variable Forcing

[27] To identify the effects of wind stress and the lateral flux on the KU intrusion, sensitivity experiments with weakening monsoonal wind stress or weakening lateral fluxes were conducted. In these experiments, winter and summer cases were run separately and the model was forced with the 7-year mean atmospheric fluxes calculated from NCEP Reanalysis data and the lateral fluxes from the Pacific Ocean model in the winter and summer, respectively. The runs were initialized with the 7-year mean *T* and *S* fields in the winter and summer from the Pacific Ocean model, respectively, and spun-up for 1000 days. Subsequently, the wind stress over entire domain (experiment 1) or the lateral momentum flux along the eastern open boundary (experiment

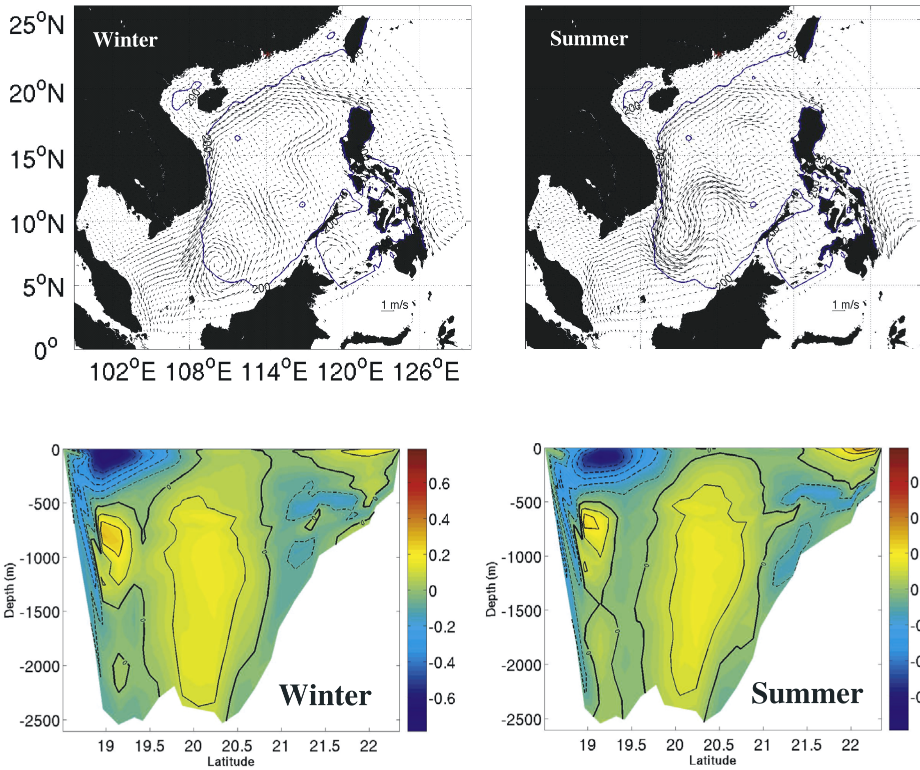


**Figure 13.** Mean surface velocity vectors (m s$^{-1}$) and mean velocity (m s$^{-1}$, positive values refer to eastward) normal to the cross section in the Luzon Strait for the case forced with weakening NEC in (left) winter and (right) summer, respectively.

2) was linearly decreased to zero from day 1000 to day 1250. The outputs averaged from day 1150 to day 1250 are presented in Figures 12 and 13.

### 5.1. Effect of Wind Forcing: Experiment 1

[28] With the weakening of the monsoonal wind stress, the strength of the winter cyclonic and summer anticyclonic circulations as well as the eddies inside the SCS are greatly reduced (Figure 12). The characteristics of the KU generally remain the same as those obtained under normal wind-forcing conditions (Figure 5a). The vertical flow structures across the Luzon Strait in both the winter and summer are very similar to those shown in Figure 8b. During weakening of the winter northeasterly wind from day 1150–1250, analysis shows that the westward intrusion of the KU in the upper layer southwest of Taiwan remains similar to the normal case. In the summer as the prevailing summer northeastward winds is weakening, a westward intrusion also occurs at the upper layer southwest of Taiwan. These findings suggest that the circulation inside the SCS is mainly forced by the monsoonal wind stress and the dynamic conditions induced by the winter/summer monsoon are favorable/unfavorable for the westward intrusion of KU.

### 5.2. Effect of the Lateral Flux in the Eastern Boundary: Experiment 2

[29] A weakening NEC, as the momentum flux in the eastern open boundary is linearly decreasing, leads to a reduction in the KU magnitude (Figure 13). The KU gradually weakens and eventually there is not enough inertia for the KU to overshoot into the Luzon Strait. As a result, the KU turns westward at the northern tip of the Philippine Islands and intrudes into the SCS. Under this condition, cyclonic circulation prevails in the SCS in both the winter and summer. An anticyclonic eddy is formed west of the Luzon Strait in both seasons, with stronger intensity in the winter. Many previous studies have also identified the existence of this eddy [e.g., *Li et al.*, 1998]. Experiment 2 illustrates that the weakening of the KU leads to a stronger KU intrusion from the southern part of the Luzon Strait and to the formation of an anticyclonic eddy west of the Luzon Strait. These findings agree with the results from the momentum analysis that inertia of the KU is key in determining its path. In addition, the summer northeastward coastal current over the continental shelf of the NSCS is markedly reduced when the summer basin-wide anticyclonic circulation is ceased in experiment 2. This finding further confirms the similar conclusion in section 3 that the shelf circulation over the NSCS in the summer is greatly influenced by the inflow from the continental shelf west of the SCS.

## 6. Summary

[30] A three-dimensional model has been developed to simulate the circulation in the SCS. The model is forced with high-frequency, time-dependent atmospheric forcing calculated from the NCEP Reanalysis data and with time- and space-dependent lateral fluxes from a Pacific Ocean

model. A strong constraint of external fluxes is imposed on the open boundaries by utilizing an active OBC to integrate time- and space-dependent barotropic and baroclinic velocities from the Pacific Ocean model into the SCS. The responses of ocean circulation to distinct seasonal forcing regimes are described. The characteristics in the simulated circulation are found to be in good agreement with results derived from remote sensing data and from previous studies. These results show that basin-wide circulations in the winter and summer are cyclonic and anticyclonic embedded with eddies of different horizontal scales. The winter-summer-winter transitions in the flow field occur in the spring and fall, with regimes shifting first in the south and in the north for the spring and fall, respectively. The monsoonal-driven circulations in the basin are regulated by the topography near continental margin in the northern and western parts of the basin. The KU tends to separate from the northern tip of the Philippine Islands and overshoot into the Luzon Strait. After moving northwestward south of the Luzon Strait, the mainstream of KU turns eastward north of the Luzon Strait and flows along the east coast of Taiwan toward the Pacific Ocean. A branch of the KU in the upper layer is able to intrude into the SCS at the shelf break southwest of Taiwan in the winter, spring and fall. The intrusion of the KU also occurs at depths in all seasons, mainly along the continental slope of the NSCS. The flow field to the east off Vietnam plays an important role in determining the circulation in the south SCS. The southward and northward coastal jets in the winter and summer, respectively, separate from the promontory location off the Vietnam and form respective cyclonic and anticyclonic recirculation. The along coast northeastward jet in the summer may also influence the flow fields in the interior of the SCS and in the region of NSCS, depending on the strength of the eastward overshooting in the coastal jet. Analysis of the momentum balance reveals that the circulation in the SCS is generally dominant by the geostrophic balance, and strong ageostrophic component are found associated with the KU in the Luzon Strait and with the coastal jet to the east off Vietnam. After overshooting into the Luzon Strait, the inertia effect of the KU in the zonal direction is locally intensified in the northern part of the Strait and leads to the formation of centripetal acceleration for the main component of KU to turn eastward toward Pacific Ocean. Part of the KU in the upper layer intrudes into the SCS when dynamic condition induced by winter monsoon prevails in the NSCS. Unlike the intrusion of KU in the upper layer, the major driving mechanism for KU intrusion at depths is found to be associated with the net westward pressure gradient force. The separation of coastal jet to the east off the Vietnam is induced by the local wind stress field and shelf topography in the summer and the associated winter, respectively. The sensitivity study reveals that the wind field has little effect on the KU east of the Luzon Strait, and the monsoonal wind stress and the associated dynamic conditions in the winter/summer are favorable/unfavorable for the intrusion of KU. Variation in the KU strength, on the other hand, has significant impact on the KU's westward intrusion into the SCS and on the formation of an anticyclonic eddy west of the Luzon Strait.

[31] **Acknowledgments.** This research was supported by the Research Grants Council of Hong Kong under grant CERG-601204. The authors would like to thank Y. Y. Cheung and C. S. Jing for help in processing data. Thoughtful comments from reviewers are appreciated.

## References

Blumberg, A. F., and G. L. Mellor (1987), A description of a three-dimensional coastal ocean circulation model, in *Three-Dimensional Coastal Ocean Models*, *Coastal Estuarine Stud.*, vol. 4, edited by N. Heap, pp. 1–16, AGU, Washington, D. C.

Chu, P. C., N. L. Edmons, and C. W. Fan (1999), Dynamical mechanisms for the South China Sea seasonal circulation and thermohaline variabilities, *J. Phys. Oceanogr.*, *29*, 2971–2989.

Curchitser, E. N., D. B. Haidvogel, A. J. Hermann, E. L. Dobbins, T. M. Powell, and A. Kaplan (2005), Multi-scale modeling of the North Pacific Ocean: Assessment and analysis of simulated basin-scale variability, *J. Geophys. Res.*, *110*, C11021 doi:10.1029/2005JC002902.

Gan, J., and J. S. Allen (2005a), Modeling upwelling circulation off the Oregon coast, *J. Geophys. Res.*, *110*, C10S07, doi:10.1029/2004JC002692.

Gan, J. P., and J. S. Allen (2005b), On open boundary conditions in a limited-area coastal model off Oregon: Response to idealized wind forcing, *Ocean Model.*, *8*, 113–115, doi:10.1016/j.ocemod2003.12.006.

Gan, J. P., R. Ingram, and R. Greatbatch (1997), On the unsteady separation/intrusion of Gaspe Current and variability in Baie des Chaleurs, Modeling Studies, *J. Geophys. Res.*, *102*, 15,567–15,581.

Gan, J. P., L. Mysak, and D. Straub (1998), Simulation of the South Atlantic Ocean circulation and its seasonal variability, *J. Geophys. Res.*, *103*, 10,241–10,251.

Gan, J. P., J. S. Allen, and R. Samelson (2005), On open boundary conditions in a limited-area coastal model off Oregon: Response to wind forcing from regional atmosphere model, *Ocean Model.*, *8*, 155–173, doi:10.1016/j.ocemod.2003.12.007.

Farris, A., and M. Wimbush (1996), Wind-induced Kuroshio intrusion into the South China Sea, *J. Oceanogr.*, *52*, 771–784.

Hu, J. Y., H. Kawamura, H. Hong, and Y. Q. Qi (2000), A review on the currents in the South China Sea: Seasonal circulation, South China Sea warm current and Kuroshio intrusion, *J. Oceanogr.*, *56*, 607–624.

Levitus, S., and T. P. Bayer (1994a), *World Ocean Atlas*, vol. 3, *Salinity*, NOAA Atlas, 99 pp., NESDIS, U.S. Dep. of Commer., Silver Spring, Md.

Levitus, S., and T. P. Bayer (1994b), *World Ocean Atlas*, vol. 4, *Temperature*, NOAA Atlas, 117 pp., NESDIS, U.S. Dep. of Commer., Silver Spring, Md.

Li, L., and R. Wu (1989), Kuroshio's loop in the South China Sea (in Chinese with English abstract), *Taiwan Strait*, *8*(1), 89–95.

Li, L., W. D. Nowlin Jr., and J. L. Su (1998), Anticyclonic rings from the Kuroshio on the South China Sea, *Deep Sea Res., Part I*, *45*, 1469–1482.

Li, L., J. D. Xu, C. Jing, R. Wu, and X. Guo (2003), Annual variation of sea surface height, dynamic topography and circulation in the South China Sea: A TOPEX/Poseidon satellite altimetry study, *Sci. China*, *46*, 127–138.

Mellor, G. L., and T. Yamada (1982), Development of a turbulence closure model for geophysical fluid problems, *Rev. Geophys.*, *20*, 851–875.

Metzger, E. J., and H. Hurlburt (1996), Coupled dynamics of the South China Sea, the Sulu Sea, and the Pacific Ocean, *J. Geophys. Res.*, *101*(C5), 12,331–12,352.

Metzger, E. J., and H. Hurlburt (2001), The importance of high horizontal resolution and accurate coastline geometry in modeling South China Sea inflow, *Geophys. Res. Lett.*, *28*(6), 1059–1062.

Qu, T., H. Mitsudera, and T. Yamagata (2000), Intrusion of the North Pacific waters into the South China Sea, *J. Geophys. Res.*, *105*, 6415–6424.

Qu, T., and R. Lukas (2003), On the bifurcation of the North Equatorial Current in the Pacific, *J. Phys. Oceanogr.*, *33*, 5–18.

Qu, T., J. B. Griton, and J. A. Whitehead (2006), Deepwater overflow through Luzon Strait, *J. Geophys. Res.*, *111*, C01002, doi:10.1029/2005JC003139.

Shaw, P. T. (1991), The seasonal variation of the intrusion of the Philippine Sea water into the South China Sea, *J. Geophys. Res.*, *96*, 821–827.

Shaw, P. T. (1992), Shelf circulation of the southeast coast of China, *Rev. Aquat. Sci.*, *6*(1), 1–28.

Shaw, P. T., and S. Y. Chao (1994), Surface circulation in South China Sea, *Deep Sea Res., Part I*, *40*, 1663–1683.

Shchepetkin, A. F., and J. C. McWilliams (2005), The regional ocean modeling system: A split-explicit, free-surface, topography following coordinates ocean model, *Ocean Modell.*, *9*, 347–404.

Wyrtki, K. (1961), Physical oceanography of the southeast Asian waters, Scientific results of marine investigations of the South China Sea and the Gulf of Thailand, *NAGA Rep. 2*, 195 pp., Scripps Inst. of Oceanogr., La Jolla, Calif.

Xie, S., Q. Xie, D. Wang, and W. T. Liu (2003), Summer upwelling in the South China Sea and its role in regional climate variations, *J. Geophys. Res.*, *108*(C8), 3261, doi:10.1029/2003JC001867.

Xu, X. Z., Z. Qiu, and H. C. Chen (1982), The general descriptions of the horizontal circulation in the South China Sea (in Chinese with English abstract), in *Proceedings of the 1980 Symposium on Hydrometeorology of the Chinese Society of Oceanology and Limnology*, pp. 137–145, Sci. Press, Beijing.

Xue, H., F. Chai, N. Pettigrew, D. Xu, M. Shi, and J. Xu (2004), Kuroshio intrusion and the circulation in the South China Sea, *J. Geophys. Res.*, *109*, C02017, doi:10.1029/2002JC001724.

Yaremchuk, M., and T. Qu (2005), Seasonal variability of the large-scale current near the coast of the Philippines, *J. Phys. Oceanogr.*, *34*, 844–855.

E. N. Curchitser, Lamont-Doherty Earth Observatory of Columbia University, 61 Route 9W, Palisades, NY 10964, USA.

J. Gan and H. Li, Department of Mathematics and Atmospheric, Marine and Coastal Environment Program, Hong Kong University of Science and Technology, Kowloon, Hong Kong. (magan@ust.hk)

D. B. Haidvogel, Institute of Marine and Coastal Sciences, Rutgers University, 71 Dudley Road, New Brunswick, NJ 08901-8521, USA.